

Development and Evaluation of a Multistatic Ultrawideband Random Noise Radar Network

Matthew E. Nelms and Peter J. Collins
School of Electrical and Computer Engineering
Air Force Institute of Technology
Wright-Patterson AFB, Ohio 45433
Email: pcollins@ieee.org

Abstract—The AFIT noise network (NoNET) is an experimental multistatic ultrawideband random noise radar designed to produce highly accurate, highly resolved imagery of a target scene while maintaining a simple design and low probability of intercept posture. This paper covers the radar node design and processing of the bistatic channel information from a cluster of widely distributed noise radar nodes. Design and integration of a distributed and central signal and data processing architecture enables the matlab-driven signal data acquisition, digital processing and multi-sensor image fusion. Experimental evaluation of the monostatic localization performance reveals its range measurement error standard deviation is 4.8 cm with a range resolution of $87.2(\pm 5.9)$ cm. AFIT's RCS range provides a clutter free joint coverage area for single and multi-target scenarios for assessing the 16-channel multistatic solution. The average multistatic localization error is assessed as $7.7(\pm 3.1)$ cm and a comparative analysis is performed against the netted monostatic solution.

I. INTRODUCTION

New research in multistatic radar systems is demonstrating the potential detection and estimation gains created by multi-transmitter, multi-receiver shared coverage areas. Spatial diversity in a distributed active sensor system has been shown to reduce the impact of target fading due to propagation factors, target scintillation and glint, and even lessen the effectiveness of certain stealth techniques [1], [2]. Additionally, the angle diversity can dramatically reduce the geometric dilution of parameters being estimated. However, such multistatic gains are not realized without a price. The overarching problem with the multistatic design is the level of complexity that results from things like hybrid distributed/central processing architectures, distributed control and supporting data-link infrastructures, and adverse mutual interference effects within the shared electromagnetic spectrum. The question becomes, what fidelity of distributed estimation (i.e. accuracy and resolution of target parameter estimation) can be obtained while still maintaining a simplistic design. It is a classic engineering problem.

Previous research at AFIT focused on the initial design and construction of an ultrawideband random noise (UWB-RN) radar network. Following the design of the digital implementation in [3], a network of three UWB-RN radars was built and qualitatively tested as a “through-the-wall” (TTW) imaging system [4]. Our current research continues this work to quantitatively determine whether a radar that uses a truly random transmit waveform coupled with a simple direct-conversion,

digital correlation receiver design is a viable architecture for covert, multistatic operations. Furthermore, characterization of the single node radar at an operating level, and evaluation of the monostatic measurement performance demonstrates whether measurement fidelity will allow an accurate central multilateration of a target scene. We analyze the results of downrange monostatic and multistatic measurements using up to six radar nodes to assess the system's performance in localizing and discriminating between multiple targets in both range and cross-range.

II. SYSTEM DESIGN AND CHARACTERIZATION

A. System Overview and Performance Metrics

System characterization is the focus of the initial design of experiments. Like all radar receivers, the basic receiver operating characteristics of the noise radar constitute the aggregate response of the receive chain hardware components. Effective calibrations insure a linear system response, predictable receiver noise power spectral densities, and accurate receiver processing conversion from correlation sample space to the downrange domain. These initial experiments are used to verify theoretical and documented receiver front-end performance, inclusive of the A/D thermal and quantization noise characteristics. This includes analysis of the power spectral densities and second-order statistics of the noise along the receive chain followed by total system response measurements in its nominal operating environment. The full system response measurements and subsequent range calibrations are designed for two reasons. The first is to establish input power calibration procedures insuring appropriate linear use of the receiver's dynamic range and accurate conversion of the target response to a time-delay domain via a two point range calibration. The second purpose is to measure the received signal bandwidth and calibrated target response SNR for use in the theoretical range resolution and range accuracy performance computations.

An example of the spectral and statistical results of the measured response of one of the NoNet radar nodes is shown in Figure 1. We note the power spectrum estimate plotted in Figure 1(a) is of significant interest in that it represents the receive signal bandwidth of the end-to-end system response. By capturing and analyzing this response using the identical spectral estimation hardware and digital signal processing

algorithms used in the direct-conversion, digital correlation receiver, more realistic predictions in the radar's performance can be made. Using a 3-dB cut-off bandwidth criteria (as opposed to the 10-dB roll-off standard used for channel isolation purposes), the effective receive signal bandwidth is found to be 185 MHz centered at 430 MHz.

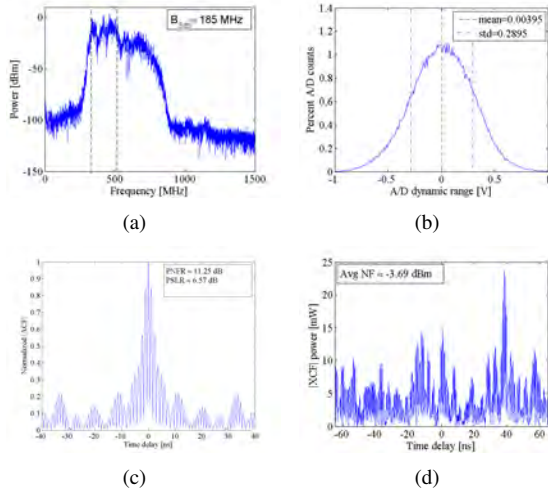


Fig. 1. System Response and statistical analysis data of characterization measurement $P0_3$ are collected using the radar's digital receiver processor as the instrumentation device. Subfigure (a) is the single-sided spectrum estimate and (b) is the histogram of percentage of A/D counts with respect to the quantized dynamic range. Subfigure (c) is a plot of the normalized $|ACF|$ of the receive channel computed using the full $1 \mu s$ record but only showing the central -40 to 40 ns discrete time delays. The data's PNFR and PSLR are annotated. Time delays from -65 to 65 ns of the two A/D channel's $|XCF|$ is similarly plotted in (d) and reveal larger than expected correlations and average noise floor.

One other important observation is made during this measurement. By varying the elevation and elevation angle of the transmit and receive antenna, it is found that the close-in clutter (specifically, the antenna spillover) increases the received signal power in such a way as to cause clipping by the A/D at its peak voltage input range of -1 to 1 V. The transmit-to-receive antenna RF spillover is a known limitation in noise modulated CW systems. By adding 3 dB of attenuation at the input to the receiver RF front-end, the A/D clipping is mitigated while maintaining a proper fill in the dynamic range as seen in Figure 1(b) (std=0.2895 V). This depth of quantization effectively uses the 8-bits for band-limited Gaussian input signals.

Finally Figures 1(c) and 1(d) establish the peak correlation side lobe and noise floor levels limiting detection performance. Further characterization measurements established the final power calibrations in the multistatic configuration including all potential signals from the multistatic receiver channels, less the actual target signal. The results highlight the challenge now left to the multistatic receiver processor - isolating a relatively weak target scattered noise signal from a strong mixture of interfering noise signals.

III. MONOSTATIC LOCALIZATION PERFORMANCE

A. Theoretical Range Accuracy Bound

Borrowed from information theory, the Cramér-Rao Lower Bound (CRLB) is a common method used in estimating various theoretical performance limits of sensors, including radars. By choosing a single measurement parameter of an unbiased estimator, τ (here set as the two-way time delay to a target) the CRLB estimates the lowest attainable variance in the error of that time delay measurement for a given system. The CRLB is an application of the Fisher Information Matrix (FIM), which defines the estimation fidelity of a set of desired parameters, based on the measurement's orthogonal sensitivity to a set of nuisance, that is, interfering parameters. Specifically, this lower bounded inequality of the error variance is the inverse of the determinant of the FIM, $|J(\Phi)|^{-1}$, such that [5]

$$\text{CRLB} = E[\hat{\tau} - \tau^2] \geq \frac{1}{|J(\Phi)|}, \quad (1)$$

where Φ is a vector of the parameters to be estimated. If $\mathbf{z}(\Phi)$ is the measured data taken by the system, it is assumed to be corrupted by various sources and types of interference, like clutter, internal thermal noise, or even external jamming signals. Because the FIM is the expected sensitivity of the measured data's probability density, $p(\mathbf{z}(\Phi))$ with respect to a change in the parameters of interest, it can be modeled as [5]

$$J(\Phi) = E \left[\left(\frac{\partial}{\partial \Phi} \log p(\mathbf{z}(\Phi)) \right) \left(\frac{\partial}{\partial \Phi} \log p(\mathbf{z}(\Phi)) \right)^T \right]. \quad (2)$$

Bernfeld and Cook point out the obvious complication in Equation 2, which requires the *a priori* probability density functions of the parameters being estimated in the measurement [6]. However, it is often valid to assume the aggregate of all interferers be modeled as zero mean white Gaussian noise (as is the case for a radar receiver that is thermal noise limited). Therefore, when envelope detection from a matched filter is employed, the theory presented in [6] reduces the error variance model for a monostatic time-delay measurement into the form

$$E[(\hat{\tau} - \tau)^2] \geq \frac{1}{B_{rms}^2 (2E/N_o)}, \quad (3)$$

a relationship with two known measurement attributes: the signal energy to noise spectral density ratio, E/N_o and an RMS bandwidth parameter, B_{rms} . The signal's B_{rms} is defined by [7]

$$B_{rms} = \sqrt{\frac{\int_{-\infty}^{\infty} (2\pi f)^2 |S(f)|^2 df}{\int_{-\infty}^{\infty} |S(f)|^2 df}}, \quad (4)$$

where $S(f)$ constitutes the voltage signal spectrum of the desired signal energy passed by the receiver front-end. As modeled by Equation 4, the spectral shape of the transmit waveform will govern the value of B_{rms} . Where a waveform of near-uniform spectral density is employed, like the rectangular shape of a B band-limited white noise, B_{rms} is approximately equal to $\pi B/\sqrt{3}$ or $1.81B$ [6].

In the context of radar performance, the more commonly used notation is the standard deviation of the time delay measurement error, σ_τ . Therefore, Equation 3 can be expressed as [7]

$$\sigma_\tau \geq \frac{1}{B_{rms} \sqrt{2 \frac{E}{N_o}}} \quad (5)$$

It is important to note that this relationship is the optimum estimation. A common practice is to estimate the accuracy based on the expected E/N_o in a particular target/clutter engagement. This expected E/N_o is similar to the threshold set for declaring a target detection and the common practice in target tracking and sensor fusion algorithms. The characterization experiments detailed in the following sections measure the expected system response and nominal E/N_o for the AFIT NoNET, which is used in predicting the system's range accuracy.

B. Monostatic Range Accuracy

Using a single radar node, a series of monostatic measurements are taken. Two dihedral corner reflectors serve as targets. Figure 2 shows the physical layout of the experiment. Initially, the upper dihedral is stacked vertically aligned with the lower dihedral, allowing for a co-range measurement. With each subsequent trial, the upper dihedral is repositioned at approximately 12.5 centimeter steps increasing in downrange distance from the radar. The resolvability assessment is based on the half-power resolution criteria, which requires a discernible 3-dB roll-off between target peaks to declare the targets resolved [6].

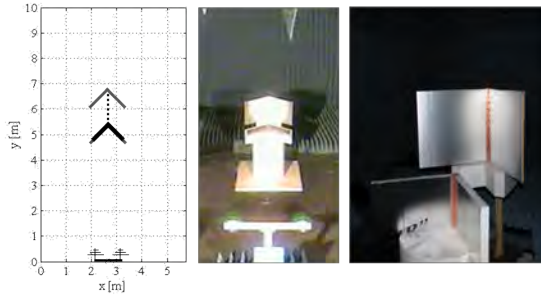


Fig. 2. Experimental set-up of the monostatic range resolution measurements with both a top view of the experiment layout in the AFIT RCS Range and photo of the actual target scenario.

The system response results of the characterization experiment found the effective bandwidth of the signal to be 185 MHz. Using the theoretical range resolution, ΔR is predicted to be 81.0 cm. Figure 3 shows four progressive plots capturing the downrange monostatic target response as the two targets in the scene become resolvable.

As expected the range ambiguity theory of two targets unresolved in range is demonstrated in Figures 3(a) and 3(b), where the dihedrals are only separated downrange first by 27.6, then by 78.5 cm. As the position of the top dihedral is incremented in range, the point at which a half-power

resolution (with respect to truth data) is obtained at 87.2(± 0.8) cm and is shown in Figure 3(c). Figure 3(d) then shows a subsequent measurement, when the targets are fully resolved to the noise floor.

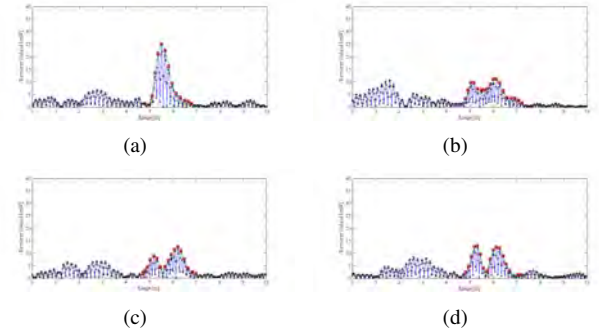


Fig. 3. Monostatic range resolution results without clutter suppression when dihedral-1 and dihedral-2 are separated by a true distance of (a) 27.6(± 0.8) cm when the skirts of their main peaks still combine with enough power to maintain a single smooth peak, (b) 78.5(± 0.8) cm and prior to being resolved, (c) 87.2(± 0.8) cm at the point of being resolved with respect to the half-power criteria, and (d) 92.7(± 0.8) cm demonstrating fully resolved targets.

The primary objective of the next experiment is to assess the monostatic range accuracy of an individual sensor. In this series of experimental trials, a monostatic radar node is used to measure the downrange location of a dihedral. To gather the necessary statistical data to compute the accuracy in terms of an error standard deviation, the dihedral is maintained in a single position for a portion of the trials. Figure 4 depicts the range configuration used to obtain the range accuracy data.

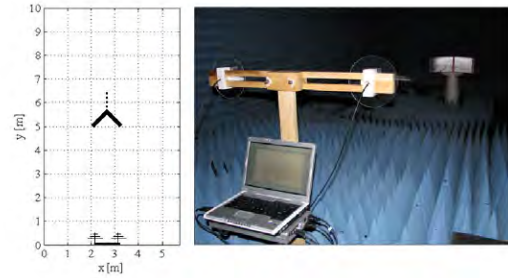


Fig. 4. Experimental set-up of the monostatic range accuracy measurements with both a top view of the experiment layout in the AFIT RCS Range and photo of the actual target scenario.

Table I contains the monostatic range accuracy measurement results for both the post-processed (clutter suppression and peak detection) measurement, MEAS*, and the measured peak detection without background subtraction, MEAS. The target location truth data represents the average of three measurements per trial taken with a calibrated laser ranging device. The results are consistent with the expected uncertainty present in radar range measurements, demonstrated by the existence of random-like error in the measurements.

Of great interest is a comparison with the predicted lower bound of the range accuracy. It is found that the standard

TABLE I
MONOSTATIC RANGE ACCURACY MEASUREMENT RESULTS

Run	dihedral (m)	MEAS* (m)	MEAS (m)
acc1	5.674	5.678	5.753
acc2	5.723	5.754	5.801
acc3a	5.774	5.757	5.701
acc3b	5.774	5.746	5.701
acc3c	5.774	5.831	5.706
acc3d	5.774	5.752	5.685
acc3e	5.774	5.773	5.712
acc3f	5.774	5.790	5.712
acc3g	5.774	5.724	5.702
acc3h	5.774	5.781	5.701
acc3i	5.774	5.796	5.764
acc3j	5.774	5.662	5.681
acc3k	5.774	5.841	5.755
acc4	5.825	5.860	5.821
acc5	5.871	5.830	5.807
acc6	5.922	5.924	5.925
acc7	6.412	6.398	6.437

deviation of the measurement error satisfies the CRLB-derived inequality given by Equation 5. Figure 5 is a graph of the *acc3* measurements from Table I converted to the measured time delay, where the standard deviation of time delay error, σ_τ , is found to be 0.319 ns (or 4.78 cm). For direct comparison of the predicted vs measured accuracy performance, the graph shows the measured data statistics plotted along with the measurement truth data and CRLB predicted time delay error. Furthermore, a negative (early) mean error bias of -37 ps (or -0.55 cm) is measured. When not utilizing the clutter suppression, σ_τ of the measured data is 0.453 ns (or 6.79 cm), and shows a positive mean error bias of +0.422 ns (or +6.32 cm).

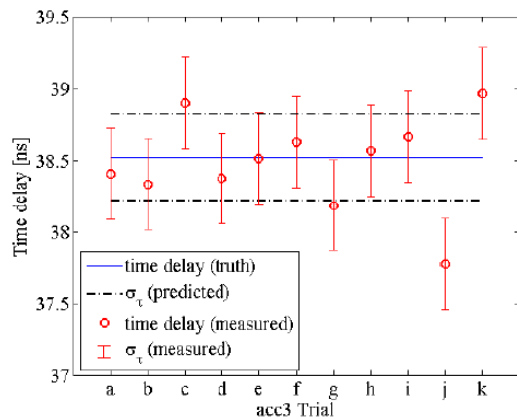


Fig. 5. Plot of the range accuracy results of the *acc3* trials presented in time delay units. Included for comparison, the error bars show the measured and CRLB-predicted standard deviations of the time delay error. Though not shown in the figure, the truth data gathered with the laser ranging device has an experimentally computed standard deviation of ± 0.39 cm (or 0.03 ns in time delay units).

IV. MULTISTATIC LOCALIZATION PERFORMANCE

The results of the multistatic experiments are evaluated to assess the 2-dimensional localization performance of the

AFIT NoNET when operating with four radar nodes. Post-processing, including clutter suppression via background subtraction and digital envelope filtering, is implemented on the data for each individual multistatic channel prior to converting the downrange profile to the referenced 2-D coordinate plane formed by the AFIT RCS chamber (See Figure 6).

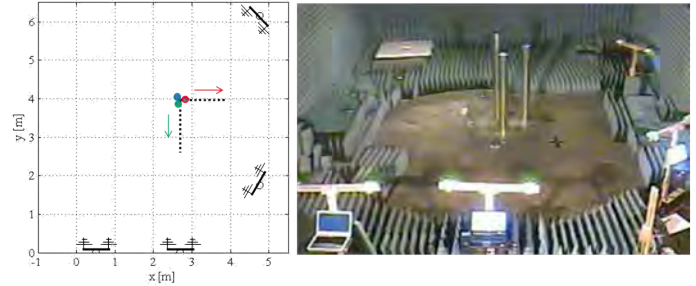


Fig. 6. Experimental set-up of the multistatic resolution measurements, with both a top view of the experiment layout in the AFIT RCS Range and photo of the actual target scenario.

Using the geometry computations and knowledge of each node's position, the multistatic isorange response is mapped into the chamber coordinate plane at the central processor, translating and rotating each channel's isorange contours as necessary. An example of the array of 2-dimensional images formed from each discrete channel is seen in Figure 7.

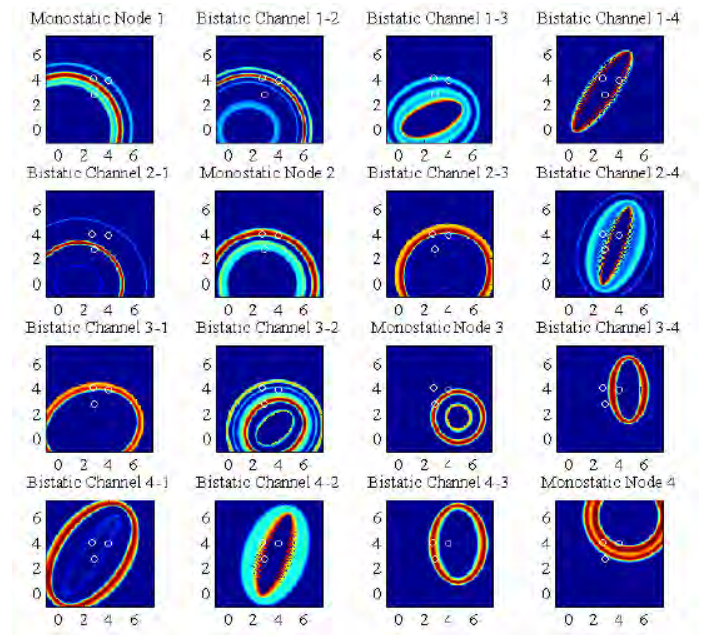


Fig. 7. An example array of the discrete images showing each of the available 16 multistatic channels prior to central processing fusion. Target locations are represented by white circles.

The multilateration image fusion technique invokes the linear combination function available as part of the Image Processing Toolbox in Matlab R2009a. The full multistatic image consists of a linear combination of the 4 monostatic

images and 12 bistatic images. To compare the results to another common form of distributed radar systems, results are also presented for the netted monostatic response, where only the 4 monostatic channels are linearly combined to form the image product. To be clear, the same data collected from each trial is being processed in two different capacities; the multistatic central processing fuses the additional bistatic channels with the monostatic channels (those being used by the netted monostatic processing).

The multistatic images seen in Figures 8 and 9 demonstrate the target resolution capabilities of the AFIT NoNET and are used to assess the range and cross-range resolution performance of the configuration. For a comparative analysis, the corresponding netted monostatic imagery is also shown. For each type of processing, the imagery products are displayed with an intentionally dynamic colormap power scale using the built-in `caxis` functions in Matlab. In general, implementing a continuous false alarm rate (CFAR) algorithm in the image fusion processing would allow a more dynamic thresholding, and therefore impact the resolution assessment. Here, the dynamic scaling is used to aid in assessing the half-power target resolution criteria. The maximum of the scale is set by the highest power level and the minimum set by an estimate of the average noise floor for that image (a basic CFAR-like post-processing).

Based on a strict half-power resolution criteria, downrange discrimination between cylinder-1 and cylinder-2 does not occur until Trial 5 for both the multistatic and netted monostatic processing, where the targets are separated by approximately 1.45 m. Cross-range discrimination is only attained with the netted monostatic configuration during Trial 4, when cylinder-1 and cylinder-3 are separated by approximately 1.29 m. Although obvious multiple target peaks exist and are clearly discernible in the imagery, the multistatic configuration does not achieve a cross-range resolution of cylinder-1 and cylinder-3 as defined by the half-power criteria. If a more robust CFAR algorithm were implemented, or simply an intelligent qualitative assessment of the imagery, the targets are discernible for the multistatic processing in Trial 4. This pertains to a cross-range resolution of approximately 1.29 m, like that of the netted monostatic.

V. CONCLUSION

The primary objectives of developing and evaluating the multistatic AFIT noise network (NoNET) were achieved by successfully demonstrating and assessing the target localization accuracy and resolution of both the system and system of systems. The major contribution of this research is the successful collection, multistatic processing and central fusion of all 16 available signal channels. It represents AFIT's first-ever distributed sensing capability using a network of active UWB-RN radars, specifically designed to exploit the bistatic channels of the system.

REFERENCES

- [1] Nicholas J. Willis and H. Griffiths, *Advances in bistatic radar*, Raleigh, NC: SciTech Pub., 2007.

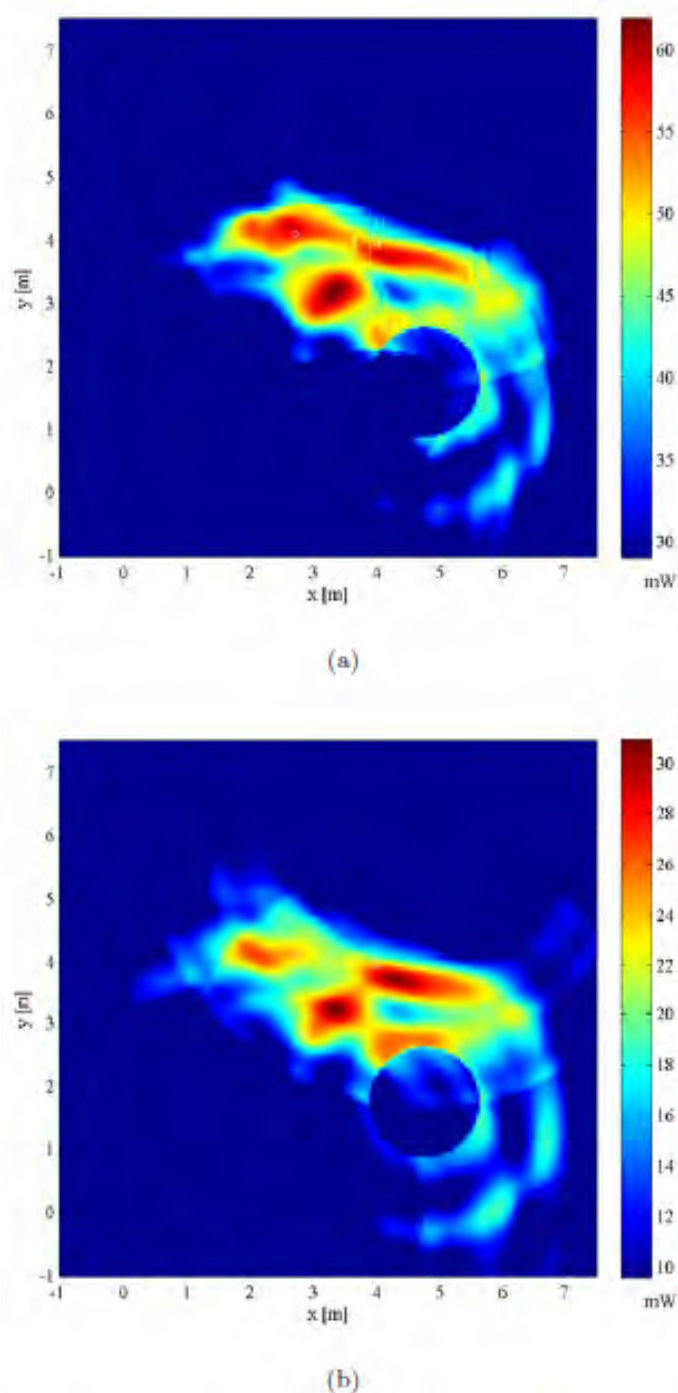
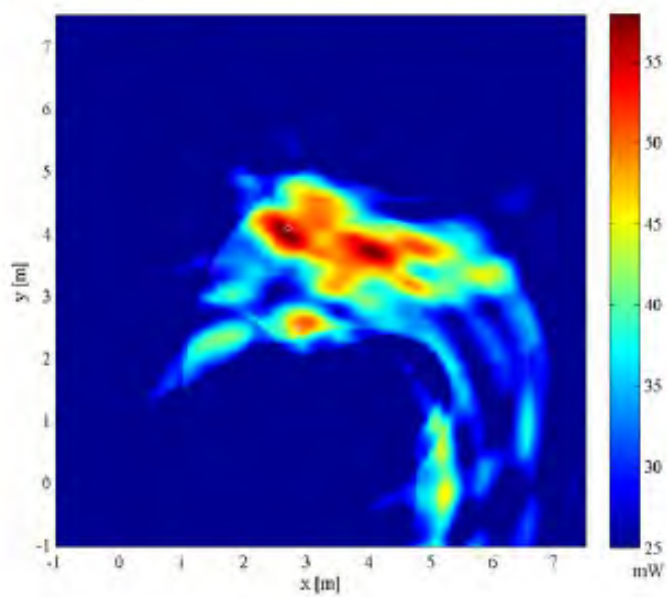
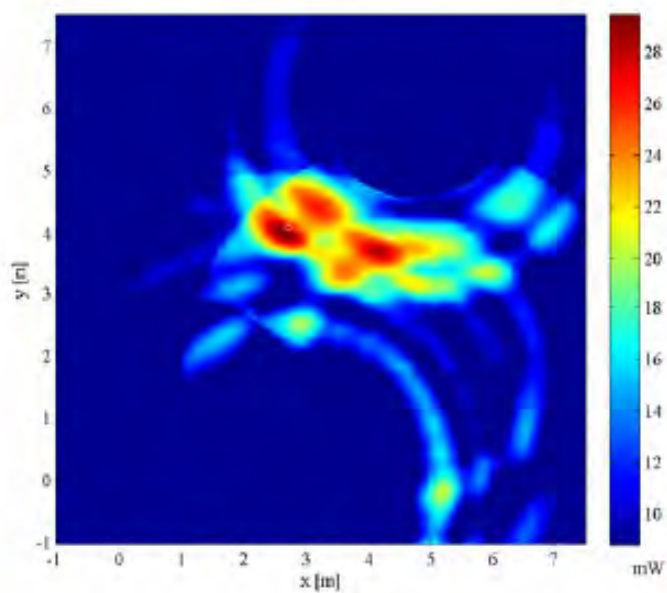


Fig. 8. Experiment *P3res4* (Trial 4) imagery products of the (a) multistatic and (b) netted monostatic measurements used to assess the range and cross-range accuracy of the AFIT NoNET.

- [2] Jian Li and Petre Stoica, *MIMO radar signal processing*, Hoboken, NJ: J. Wiley & Sons, 2009.
- [3] C. P. Lai, *Through Wall Surveillance Using Ultrawideband Random Noise Radar*, PhD dissertation. Pennsylvania State University, University Park, PA, 2007.
- [4] Schmitt, A. and Collins, P.J., *Demonstration of a Network of Simultaneously Operating Digital Noise Radars*, IEEE Antennas and Propagation Magazine, Vol. 51, No. 2, pp. 125–130, April 2009.
- [5] Louis L. Scharf and Cdric Demeure, *Statistical signal processing :de-*



(a)



(b)

Fig. 9. Experiment *P3res5* (Trial 5) imagery products of the (a) multistatic and (b) netted monostatic measurements used to assess the range and cross-range accuracy of the AFIT NoNET.

tection, estimation, and time series analysis, Reading, Mass.:Addison-Wesley Pub. Co., 1991.

[6] Charles E. Cook and Marvin Bernfeld, *Radar signals;an introduction to theory and application*, New York:Academic Press, 1967.

[7] David Knox Barton, *Radar system analysis and modeling*, Boston, MA:Artech House, 2004.